

Unidirectional Nonlinear \mathcal{PT} -symmetric Optical Structures

Hamidreza Ramezani¹ and Tsampikos Kottos^{1,2}

¹*Department of Physics, Wesleyan University, Middletown, Connecticut 06459, USA*

²*Max-Planck-Institute for Dynamics and Self-Organization, 37073Göttingen, Germany*

Ramy El-Ganainy and Demetrios N. Christodoulides

College of Optics & Photonics-CREOL, University of Central Florida, Orlando, Florida 32816, USA

(Dated: October 22, 2018)

We show that non-linear optical structures involving a balanced gain-loss profile, can act as unidirectional optical valves. This is made possible by exploiting the interplay between the fundamental symmetries of parity (\mathcal{P}) and time (\mathcal{T}), with optical nonlinear effects. This novel unidirectional dynamics is specifically demonstrated for the case of an integrable \mathcal{PT} -symmetric nonlinear system.

PACS numbers: 42.25.Bs, 11.30.Er, 42.82.Et

I. INTRODUCTION

Transport phenomena and in particular directed transport are at the heart of many fundamental problems in physics, chemistry and biology [1]. At the same time they are also of great relevance to technological applications based on a variety of transport-based devices such as rectifiers, pumps, particle separators, molecular switches, and electronic diodes and transistors. Of special interest is the realization of novel classes of integrated photonic devices that allow one-directional flow of information-e.g. optical isolators [2]. Currently, such unidirectional elements rely mainly on the Faraday effect, where external magnetic fields are used to break the space-time symmetry. This in general requires materials with appreciable Verdet constants-typically non compatible with light-emitting wafers [2]. To anticipate these problems, alternative proposals for the creation of optical diodes and isolators have been suggested in recent years. Some representative examples include the creation of optical diodes based on asymmetric nonlinear absorption [3], second harmonic generation in asymmetric waveguides [4], nonlinear photonic crystals [5], and photonic quasi-crystals and molecules [6].

In this paper, we propose a new mechanism for unidirectional optical transport based on configurations involving nonlinear optical materials with Parity (\mathcal{P}) and Time (\mathcal{T})-reflection. This is possible by judiciously interleaving gain and loss regions, in such a way that the (complex) refractive index $n(x) = n_R(x) + i\gamma n_I(x)$ profile satisfies the condition $n^*(-x) = n(x)$. A first experimental realization of such (linear) arrangements has been recently reported in Refs. [7, 8] where a \mathcal{PT} dual coupled structure was fabricated and the beam dynamics was investigated. Here we show that the interplay of non-reciprocal dynamics arising from \mathcal{PT} -symmetry [8], and self-trapping phenomena associated with Kerr nonlinearities [9], can mold the flow of light in a surprising way. Such novel directed dynamics can be exploited in the realization of a new generation of optical isolators or diodes.

Even though the validity of our arguments can be demonstrated for a variety of non-linear \mathcal{PT} -configurations, below, we will highlight its basic principles, using the simplest possible arrangement, consisting of two \mathcal{PT} -coupled waveguide elements with Kerr nonlinearity of strength χ . Each of the waveguides is single-moded- one providing gain and the other an equal amount of loss (see Fig. 2). We have obtained the phase diagram in the $\chi - \gamma$ plane for which our system acts as an optical diode, and we have identified the minimum propagation length needed, in order to achieve this unidirectional functionality. Detail numerical simulations support our theoretical predictions.

This paper is structured as follows. In Sec. II an overview of the linear \mathcal{PT} -symmetric dimer is presented. The nonlinear \mathcal{PT} -symmetric dimer will be introduced in Sec. III, where the equations of motion are given in terms of Stokes parameters. In subsection III.A, we present both our theoretical and numerical results on the dynamics of the non-linear \mathcal{PT} -symmetric dimer. In subsection III.B we calculate the critical value of the non-linearity for which diode action is possible. Finally we will draw our conclusions in Sec. IV.

II. LINEAR \mathcal{PT} -SYMMETRIC DIMER: AN OVERVIEW

In this section we will briefly review the basic properties of the linear \mathcal{PT} -symmetric dimer [7, 8, 11]. In integrated optics this simple \mathcal{PT} element can be realized in the form of a coupled system, with only one of the two parallel channels being optically pumped to provide gain γ for the guided light, whereas the neighbour arm experiences equal amount of loss (see Fig. 1). Under these conditions, and by using the coupled-mode approach, the optical-field dynamics in the two coupled waveguides are described by the following set of equations:

$$\begin{aligned} i \frac{d\psi_1}{dz} + \psi_2 - i\gamma\psi_1 &= 0; & (a) \\ i \frac{d\psi_2}{dz} + \psi_1 + i\gamma\psi_2 &= 0; & (b) \end{aligned} \quad (1)$$

where $\psi_{1,2}$ are modal electric field amplitudes in the amplifying (Eq. 1a) and lossy (Eq. 1b) waveguide channels, z represents a dimensionless propagation distance- normalized in units of coupling lengths, and γ is a scaled gain/loss coefficient, also normalized to the coupling strength.

The Hamiltonian corresponding to the linear problem of Eq. (1), is written as:

$$\mathcal{H} = \begin{pmatrix} i\gamma & -1 \\ -1 & -i\gamma \end{pmatrix} \quad (2)$$

and commutes with the combined \mathcal{PT} operator. A surprising result associated with this class of problems is the possibility that such a \mathcal{PT} symmetric Hamiltonian \mathcal{H} can have an entirely real energy spectrum, despite the fact that, in general, they are non-Hermitian [7, 8, 11–20]. For the specific example of the non-hermitian Hamiltonian of Eq. (2), a direct diagonalization gives the following set of eigenvalues:

$$\lambda_{\pm} = \pm \sqrt{1 - \gamma^2} \quad (3)$$

which are real as long as the gain/loss parameter γ is smaller than some critical value, $\gamma_{\mathcal{PT}} = 1$ (*exact \mathcal{PT} -symmetric phase*). As the gain/loss parameter γ increases above $\gamma_{\mathcal{PT}}$, the eigenvalues becomes complex (*broken \mathcal{PT} -symmetric phase*). The corresponding eigenvectors of the Hamiltonian Eq. (2) are

$$|+\rangle = \begin{pmatrix} e^{i\frac{\alpha}{2}} \\ e^{-i\frac{\alpha}{2}} \end{pmatrix}, |-\rangle = \begin{pmatrix} ie^{-i\frac{\alpha}{2}} \\ -ie^{i\frac{\alpha}{2}} \end{pmatrix}; \sin \alpha = \gamma \quad (4)$$

In the exact \mathcal{PT} -symmetric phase, both the \mathcal{H} and \mathcal{PT} operators share the same set of eigenvectors. In this regime, the mode intensity is symmetric with respect to the mirror axis of the two waveguides. As γ increases above $\gamma_{\mathcal{PT}}$ the eigenfunctions of \mathcal{H} cease to be eigenfunctions of the \mathcal{PT} -operator, despite the fact that \mathcal{H} and the \mathcal{PT} -operator still commute. This happens because the \mathcal{PT} -operator is anti-linear, and thus the eigenstates of \mathcal{H} may or may not be eigenstates of \mathcal{PT} . In the broken \mathcal{PT} -symmetric phase, the spacial distribution of the modes is asymmetric, one of them living predominantly in the amplifying waveguide and the other in the lossy one. At the phase-transition point $\gamma = \gamma_{\mathcal{PT}}$ the two eigenfunctions and their corresponding eigenvalues coalesce leading to an “exceptional” point singularity [21].

The beam dynamics associated with Eq. (1) were investigated theoretically in Refs. [7, 11, 12] while direct measurements were performed in [7, 8]. These authors recognized that as the gain/loss parameter γ reaches $\gamma_{\mathcal{PT}}$, the total beam power starts growing exponentially, while for $\gamma < \gamma_{\mathcal{PT}}$ power oscillations are observed (see Figs. 1b,c). The most dramatic effect in the beam evolution is the appearance of non-reciprocal wave propagation (see Figs. 1c-f). Specifically, the beam propagation pattern differs depending on whether the initial excitation is on the left or right waveguide. This is contrasted with the $\gamma = 0$ case (Fig. 1a,b), where the beam propagation is insensitive to the initial condition.

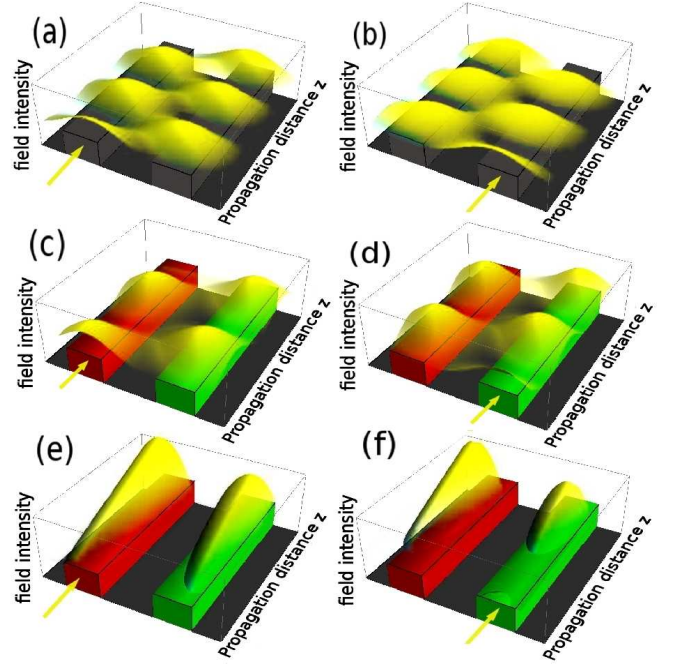


FIG. 1. (color online) Beam propagation in two coupled linear waveguides. For the parameters of the simulation (we use normalized coupling units), the spontaneous \mathcal{PT} -breaking take place at $\gamma_{\mathcal{PT}} = 1$. In all cases, left (right) panels correspond to an initial excitation at the left (right) channel. (a,b) A passive system corresponding to $\gamma = 0$. The propagation is reciprocal; (c,d) $\gamma = 0.4\gamma_{\mathcal{PT}}$ corresponding to the exact \mathcal{PT} -phase. A non-reciprocal beam propagation is evident. Although the dynamics is non-Hermitian, the evolution is “pseudo-unitary” and the total beam power remains bounded; (e,f) For $\gamma = 1.5\gamma_{\mathcal{PT}}$, beam power grows exponentially (vertical scale is logarithmic) in both waveguides, while the beam propagation is again non-reciprocal with respect to the mirror axis of the two waveguides. Waveguides are color-coded, indicating balanced gain (red) and loss (green) regions. Grey-color waveguides indicate a passive ($\gamma = 0$) system.

III. NON-LINEAR \mathcal{PT} -SYMMETRIC DIMER

We begin our analysis by providing the mathematical model that describes optical wave propagation in a Kerr nonlinear \mathcal{PT} symmetric coupled dual waveguide arrangement (see Fig. 2). The two modal field amplitudes are governed by the evolution equations:

$$\begin{aligned} i \frac{d\psi_1}{dz} + \psi_2 - i\gamma\psi_1 + \chi|\psi_1|^2\psi_1 &= 0; & (a) \\ i \frac{d\psi_2}{dz} + \psi_1 + i\gamma\psi_2 + \chi|\psi_2|^2\psi_2 &= 0; & (b) \end{aligned} \quad (5)$$

where χ is the strength of the Kerr-nonlinearity.

Equations (5) can be rewritten in terms of the (real) Stokes parameters $S_i = \psi^\dagger \hat{\sigma}_i \psi$, where $\hat{\sigma}_i$ ($i = 0, 1, 2, 3$) denote the Pauli spin matrices [22]. In this representation, the total field intensity is given by $S_0 = |\psi_1|^2 + |\psi_2|^2$, $S_3 = |\psi_1|^2 - |\psi_2|^2$ is the intensity imbalance between the two waveguides, while $S_1 = \psi_1^* \psi_2 + \psi_1 \psi_2^*$ and $S_2 =$

$i(\psi_1\psi_2^* - \psi_1^*\psi_2)$. In this representation Eqs. (5) take the form:

$$\frac{dS_0}{dz} = \vec{E} \cdot \vec{S}; \quad \frac{d\vec{S}}{dz} = S_0\vec{E} + \vec{S} \times \vec{B} \quad (6)$$

where we have introduced the two real vectors $\vec{E} = (0, 0, 2\gamma)$ and $\vec{B} = (2, 0, \chi S_3)$, and the 3-dimensional Stokes vector $\vec{S} \equiv (S_1, S_2, S_3)$. We note that the condition $S_0^2 - \vec{S} \cdot \vec{S} = 0$ is always satisfied. It is worth mentioning that Eqs. (6), are identical to the equation of motion of a relativistic negatively -charged particle with zero mass, in a pseudo-electromagnetic field (\vec{E}, \vec{B}) , where (S_0, \vec{S}) represents the energy and 3-dimensional momentum of the particle, while the propagation distance z has the role of the time.

Nonlinear \mathcal{PT} -symmetric optical coupled systems can be realistically synthesized on semiconductor wafers-known for their high Kerr-like nonlinearities [10]. As in Ref. [8], coupling lengths as low as $L_c = 1\text{mm}$ can be obtained, in which case a gain/loss level below $\pm 30\text{cm}^{-1}$ (readily available in such materials) will suffice to keep the arrangement in the \mathcal{PT} phase. In addition, critical switching ($\chi \sim 1$) can also occur at milliwatt power levels in multi-quantum well configurations.

A. Dynamics

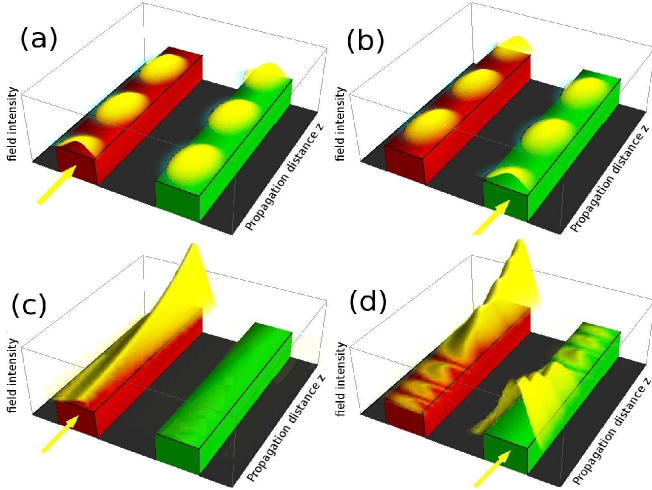


FIG. 2. (color online) Beam propagation in two coupled nonlinear waveguides with non-linearity strength χ and a complex \mathcal{PT} -symmetric refractive index profile. Waveguides are color-coded, indicating balanced gain (red) and loss (green) regions ($\gamma = 0.1$). Left columns correspond to an initial excitation at the gain waveguide port, while right columns correspond to an initial excitation at the lossy waveguide: (a,b) The non-linearity $\chi = 1.9$ is below the critical value $\chi_d \approx 3.37$ while for (c,d) the non-linearity strength $\chi = 8$ is above.

For $\gamma = 0$, Eqs. (6) admits two constants of motion: the total input power S_0 and the total energy

$\mathcal{H} = (\chi/2)S_3^2 + 2S_1$. These two constants allow for an analytic solution of the Stokes vector \vec{S} in terms of elliptic functions [9]. Depending on the initial preparation and strength of nonlinearity χ , we observe two distinct dynamical behaviors. For example, if the initial beam of total input power $S_0(0) = 1$, is prepared in one of the two waveguides (i.e. $S_3(0) = \pm 1$), we observe either Rabi oscillations, or self-trapping dynamics [9]. The former case corresponds to $\chi < 4$ and results in beam oscillations between the two waveguides, while the latter case, occurs for $\chi > 4$ and leads to localization of the field (for all times) at the waveguide that was initially placed. In both cases, symmetric initial preparation will result to a dynamics which is reciprocal with respect to the axis of symmetry of the two coupled waveguides.

For $\gamma \neq 0$, neither the energy \mathcal{H} nor the beam power S_0 are anymore conserved quantities. Nevertheless, \mathcal{PT} -symmetry enforces two other constants of motion C, J :

$$\begin{aligned} C^2 &= (\chi S_1 - 2)^2 + (\chi S_2)^2, & (a) \\ J &= S_0 + \frac{2\gamma}{\chi} \sin^{-1} \left(\frac{\chi S_1 - 2}{C} \right), & (b) \end{aligned} \quad (7)$$

thus indicating that the system of Eqs. (5) is fully integrable. Below we will consider the case where initially $S_0(0) = 1$, $S_3(0) = \pm 1$, while $S_1(0) = S_2(0) = 0$. In this case, the constants of motion, as defined in Eqs. (7), take the values $C_{\pm} = \pm 2$ and $J_{\pm} = 1 \mp \gamma\pi/\chi$.

Using C and J , in this particular case we can express the components of the Stokes vector in terms of $S_0(z)$ in the following way

$$\begin{aligned} \chi S_1 &= 2 \left(1 - \cos \left(\chi \frac{1 - S_0(z)}{2\gamma} \right) \right), & (a) \\ \chi S_2 &= 2 \sin \left(\chi \frac{1 - S_0(z)}{2\gamma} \right), & (b) \\ \chi S_3 &= \pm \sqrt{(\chi S_0(z))^2 - \left(4 \sin \left(\frac{\chi}{4\gamma} (1 - S_0(z)) \right) \right)^2}. & (c) \end{aligned} \quad (8)$$

Substituting the expression for S_3 from Eq. (8c), to the first of the Eqs. (6), we get that

$$\pm \int_{S_0=1}^{S_0(z)} \frac{dS_0}{\sqrt{(\chi S_0)^2 - \left(4 \sin \left(\frac{\chi}{4\gamma} (1 - S_0) \right) \right)^2}} = \frac{2\gamma}{\chi} z. \quad (9)$$

Even though the problem is soluble by quadratures, the integral in Eq. (9) cannot be evaluated further and thus a closed expression for $S_0(z)$ is not possible. It is therefore instructive at this point to gain insight on the properties of the dynamics of this \mathcal{PT} non-linear coupler by numerically solving Eqs. (5,6). The accuracy of the numerical integration was checked via the conservation laws Eq. (7), which were satisfied up to 10^{-10} .

Examples of the resulting beam dynamics for $\gamma = 0.1$ and two representative non-linearity strengths $\chi = 1.9$ and $\chi = 8$ are reported in Fig. 2a,b and 2c,d respectively. In contrast to the $\gamma = 0$ case [9], now the dynamics is non-reciprocal with respect to the axis of symmetry of the system. While this is true for both values

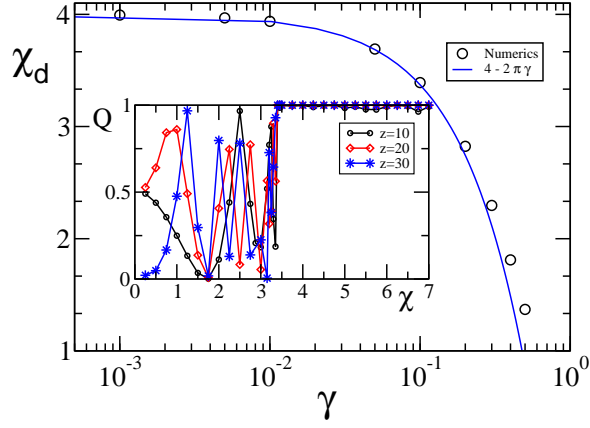


FIG. 3. (color online) Main figure: A semi-logarithmic plot of χ_d vs. γ . For the numerical evaluation of χ_d we have integrated Eq. (5) Inset: The efficiency factor Q vs. non-linearity strength χ , for a fixed gain/loss parameter $\gamma = 0.1$ and three different waveguide lengths $z = 10, 20$ and $z = 30$. For non-linearity strength $\chi = \chi_d \approx 3.4$ the isolator reaches its optimal efficiency.

of non-linearity strength χ , it is much more pronounced for the case of Figs. 2c,d. In this latter case, the output field always leaves the sample from the waveguide with gain (red-colored) irrespective of the preparation of the input beam. At the same time the output beam intensity at the lossy waveguide approaches zero for longer waveguides. It is important to stress that in the case of the linear \mathcal{PT} -dimer (see Figs 1e-f) the beam intensity at the lossy waveguide never goes to zero. Instead it increases exponentially, albeit with a smaller prefactor with respect to the one of the gain waveguide. This novel unidirectional propagation of the \mathcal{PT} -symmetric non-linear dimer is the key mechanism for establishing optical isolators (diodes). It has to be contrasted with the corresponding cases shown in Figs. 2a,b where the output beam depends on the input state, i.e. an initial excitation at the gain waveguide results in an output field at the lossy guide and vice versa.

To quantify the ability of our set-up to act as an optical non-reciprocal device, we have defined the efficiency factor Q of unidirectional propagation as

$$Q(z) = 1 - |T_{+,+}(z) - T_{-,+}(z)|. \quad (10)$$

where $T_{\pm,+}(z) \equiv |\psi_1(z)|^2/S_0(z)$ is the normalized transmission coefficient associated with the gain (+) waveguide of length z . In our definition we have always assumed that the initial input beam has total power $S_0(z=0) = 1$, while the beam is launched either in the gain (+) or in the loss (-) waveguide. The efficiency factor takes values from $0 \leq Q \leq 1$: a perfect diode corresponds to $Q = 1$ (since the term inside the absolute value in Eq. (10) will be zero), while the opposite limit of $Q = 0$ indicates total revival of the field. In the inset of Fig. 3 we report our numerical findings for the efficiency factor Q as a function of the non-linearity strength χ for

three different waveguide lengths $z = 10, 20$, and $z = 30$, and for a fixed value of the gain/loss parameter $\gamma = 0.1$. It is clear that an optimal diode is achieved once the non-linearity strength χ is larger than a critical value χ_d .

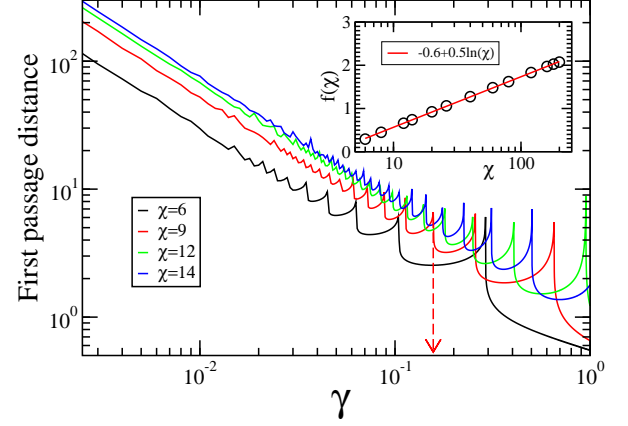


FIG. 4. (color online) The numerically extracted first passage distance z_{fpd} versus the gain/loss parameter γ . The initial conditions are chosen to be $S_0(0) = 1$ and $S_3(0) = -1$. An inverse power law is observed. Left inset: The proportionality coefficient $f(\chi)$ is plotted versus the non-linearity strength χ for $\chi > \chi_d$. The red line correspond to the best linear fit.

B. Critical Non-linearity

Next we present a heuristic argument that aims to estimate the critical non-linearity strength χ_d (as a function of γ), above which the \mathcal{PT} symmetric non-linear dimer acts as an optical diode of high efficiency factor $Q = 1$. To this end we focus our analysis on the temporal behavior of the total power $S_0(z)$. In the case of (Rabi-like) oscillations $S_0(z)$ is bounded between a minimum and a maximum value. Instead, in the regime where the coupled system acts as an optical diode, $S_0(z)$ is bounded only from below, while asymptotically it grows in an exponential fashion [23]. Using the first of Eq. (6) together with Eq. (8c), and requesting the extrema condition $dS_0(z)/dz = 0$ (which is equivalent to $S_3(z) = 0$) together with the condition $d^2S_0/dz^2 < 0$ for the existence of a global maxima, we find that $S_0(z)$ shows oscillatory behavior (i.e. Rabi-like oscillations) if the non-linearity χ is smaller than χ_d , given by

$$\chi_d = 4 - 2\pi\gamma \quad (11)$$

In the main panel of Fig. 3 we compare Eq. (11) with the numerical values found for χ_d . The latter has been evaluated via a direct integration of Eq. (5) for systems sizes up to $z = 10^6$. The critical non-linearity χ_d was evaluated up to a fourth digit accuracy as the nonlinearity strength for which the total power $S_0(z)$, is bounded. In all cases the accuracy of the integration scheme has been guaranteed by requesting that the constants of motion Eq. (7)

are conserved with accuracy up to 10^{-5} . A nice agreement between the theoretical and numerical value of χ_d is evident for small values of the gain/loss parameter γ , while deviations from the theoretical prediction start to be visible as γ approaches the \mathcal{PT} transition point (i.e. $\gamma = 1$) of the linear system.

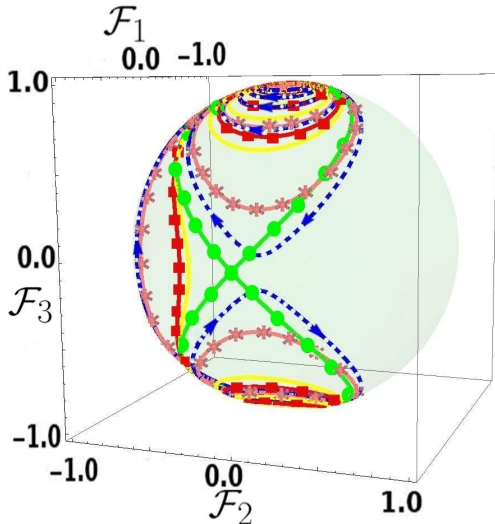


FIG. 5. (color online) Dynamics of the rescaled Stokes variables \mathcal{F} for $\chi = 9$ and various gain/loss parameters γ : dashed blue line correspond to $\gamma = 0.157$; pink line (\star) correspond to $\gamma = 0.15$; solid yellow line correspond to $\gamma = 0.12$; and red line (\blacksquare) to $\gamma = 0.174$. The green line (\bullet) corresponds to the passive system $\gamma = 0$ with critical non-linearity $\chi = 4$, where the motion of the trajectory is on the separatrix. The trajectory associated with $\gamma = 0.157$ (see red arrow in Fig. 4) is typical to the cases where z_{fpd} diverge and correspond to the closest one to the separatrix of the passive $\gamma = 0$ system.

Finally, we investigate the minimal waveguide length z_d which is required in order to have a high- Q diode. From Figs. 2c,d we see that the beam evolution follow two distinct scenaria depending on the initial conditions: if the beam is launched initially at the gain waveguide, the propagation is mainly along this channel. If on the other hand the beam excites the lossy waveguide, there is a minimum propagation distance z_d which is required before the light intensity is concentrated in the gain waveguide. We have found that z_d is proportional to the "first passage distance" z_{fpd} associated with the point that S_3 becomes zero for the first time. In Fig. 4 we report the results of our simulations for $z_d \sim z_{\text{fpd}}$ for various $\chi(>\chi_d)$ values or input power levels.

An intriguing feature of z_{fpd} is the existence of singu-

larities (peaks in the z_{fpd}) for some characteristic values of the gain/loss parameter γ . To understand the origin of these singularities, we have plotted the evolution of the Stokes vector \vec{S} , by making use of the rescaled variables $\vec{\mathcal{F}} = \vec{S}/S_0$. In this representation, the magnitude $|\vec{\mathcal{F}}|$ remains constant, and thus we can visualize the evolution on the Bloch sphere (see Fig. 5). It should be emphasized that the Bloch trajectories can in general show self-intersections, as they are a projection from a higher dimensional phase space. One must also distinguish between closed orbits and those approaching an asymptotic state, as this is in general connected to broken and unbroken \mathcal{PT} -symmetry [13]. We note that closely related Bloch dynamics appear in different physical model systems like the ones reported in [24]. Our analysis, indicated that the singularities in z_{fpd} are associated with trajectories that during their evolution, they stay close to the separatrix associated to the critical value $\chi = 4$ (transition between Rabi-oscillations and self-trapping) of the passive system.

Leaving aside the issue of the singularities, we have found that for all χ -values larger than χ_d , the first passage distance z_{fpd} follows an inverse power law i.e.

$$z_{\text{fpd}} = f(\chi)/\gamma \quad (12)$$

where the proportionality factor $f(\chi)$ is χ -dependent. A best least square fit allow us to extract the various $f(\chi)$ which is in this case $f(\chi) = -0.6 + 0.5\ln(\chi)$ (see inset of Fig. 4).

IV. CONCLUSIONS

In conclusion, we have proposed a new mechanism for directed transport in nonlinear optical coupled systems, that relies at the interplay between nonlinearity and \mathcal{PT} -reflection symmetries. More specifically, we have observed that above a critical non-linearity strength, the beam evolution is unidirectional, i.e. the output beam remains in the gain channel, irrespective of initial conditions. Such behavior implies that these systems can be used to realize new classes of optical diodes and other unidirectional photonic elements. Of great interest will be to extend these notions to more involved arrangements like nonlinear \mathcal{PT} lattices where nonlinear excitations are expected lead to even more intriguing phenomena.

We would like to acknowledge V. Kovanis for useful comments and suggestions. This work was supported by the DFG FOR760, and a grant from the US-Israel Binational Science Foundation (BSF), Jerusalem, Israel.

[1] Ch. Kittel, *Introduction to Solid State Physics*, Wiley (2005); R. D. Astumian and P. Hänggi, *Phys. Today* **55**, 33 (2002); F. Jülicher, A. Ajdari, J. Prost, *Rev. Mod.*

Phys. **69**, 1269 (1997); P. Reimann, *Phys. Rep.* **361**, 57 (2002).

[2] B. E. A. Saleh and M. C. Teich, *Fundamentals of Pho-*

- tonics* (Wiley, New York, 1991).
- [3] R. Philip, M. Anija, C. S. Yelleswarapu, D. V. G. L. N. Rao, Appl. Phys. Lett. **91**, 141118 (2007).
 - [4] K. Gallo, G. Assanto, K. R. Parameswaran, M. M. Fejer, Appl. Phys. Lett. **79**, 314 (2001); K. Gallo, G. Assanto, J. Opt. Soc. Am. B **16**, 267 (1999).
 - [5] M. Scalora, J. P. Dowling, C. M. Bowden, M. J. Bloemer, J. Appl. Phys. **76**, 2023 (1994).
 - [6] F. Biancalana, J. Appl. Phys. **104**, 093113 (2008); H. Zhou, K-F. Zhu, W. Hu, Q. Guo, S. Lan, X-S. Lin, A. V. Gopal, J. Appl. Phys. **99**, 123111 (2006).
 - [7] A. Guo, et al., Phys. Rev. Lett. **103**, 093902 (2009)
 - [8] C. E. Rüter, et al., Nature Physics **6**, 192 (2010).
 - [9] S. M. Jensen, IEEE J. Q. Electron. **18**, 1580 (1982); V. M. Kenkre, D. K. Campbell, Phys. Rev. B **34**, 4959 (1986).
 - [10] P. LiKamWa, et al, Electron. Lett. **21**, 26 (1985); U. Das, Y. Chen, and P. Bhattacharya, Appl. Phys. Lett. **51**, 1679 (1987).
 - [11] T. Kottos, Nature Physics **6**, 167 (2010).
 - [12] C. M. Bender, S. Boettcher, Phys. Rev. Lett. **80**, 5243 (1998); C. M. Bender, D. C. Brody, H. F. Jones, Phys. Rev. Lett. **89**, 270401 (2002); C. M. Bender, D.C. Brody, H. F. Jones, and B. K. Meister, Phys. Rev. Lett. **98**, 040403 (2007). U. Günther and B. F. Samsonov, *ibid.* **101**, 230404 (2008).
 - [13] C. M. Bender, S. Boettcher, P. N. Meisinger, J. Math. Phys. **40**, 2201 (1999); C. M. Bender, Rep. Prog. Phys. **70**, 947 (2007); C. M. Bender, D. C. Brody, and H. F. Jones, Phys. Rev. Lett. **89** 270401 (2002).
 - [14] O. Bendix, R. Fleischmann, T. Kottos, and B. Shapiro, Phys. Rev. Lett. **103**, 030402 (2009); C. T. West, T. Kottos, T. Prosen, Phys. Rev. Lett. **104**, 054102 (2010).
 - [15] C. M. Bender, P. D. Mannheim, Phys. Rev. D **78**, 025022 (2008); C. M. Bender, G. V. Dunne, P. N. Meisinger, Phys. Lett. A **252**, 272 (1999).
 - [16] R. El-Ganainy, K. G. Makris, D. N. Christodoulides, Z. H. Musslimani, Opt. Lett. **32**, 2632 (2007).
 - [17] K. G. Makris, R. El-Ganainy, D. N. Christodoulides, Z. H. Musslimani, Phys. Rev. Lett. **100**, 103904 (2008).
 - [18] Z. H. Musslimani, K. G. Makris, R. El-Ganainy, D. N. Christodoulides, Phys. Rev. Lett. **100**, 030402 (2008).
 - [19] S. Klaiman, U. Günther, N. Moiseyev, Phys. Rev. Lett. **101**, 080402 (2008).
 - [20] S. Longhi, Phys. Rev. Lett. **103**, 123601 (2009); S. Longhi, Phys. Rev. B **80**, 235102 (2009).
 - [21] M. Berry, J. Mod. Opt. **50**, 63 (2003); M. Moiseyev, S. Friedland, Phys. Rev. A **22**, 618 (1980).
 - [22] E. Hecht, Optics, 2nd ed., Addison-Wesley (1987)
 - [23] In this case, the system of Eq. (5) act as a set of two uncoupled waveguides i.e. in the long time limit one can assume that the coupling constant is essentially zero. As a result the intensity at the gain waveguide (which is approximately the same as the total intensity) increases exponentially, while the one at the lossy waveguide decays exponentially. We have checked the accuracy of this statement with direct numerical simulations.
 - [24] E. M. Graefe, H. J. Korsch, and A. E. Niederle, Phys. Rev. Lett. **101**, 150408 (2008); S. Morrison and A. S. Parkins, Phys. Rev. Lett. **100**, 040403 (2008).